An experimental investigation of a flexible sintered silver joint for micro-joining based on a design of experiments

Laurent VIVET
VALEO
THS Material Laboratory
78321 La Verrière, France
laurent.vivet@valeo.com

Lahouari BENABOU
LISV
Université de Versailles SQY-Paris Saclay
78321 Vélizy, France
lahouari.benabou@uvsq.fr

Olivier SIMON
LISV
Université de Versailles SQY-Paris Saclay
78321 Vélizy, France
olivier .simon@uvsq.fr

***Abstract*— The increasing electrification of vehicles requires the use of ever higher voltages and electrical power. The thermal stresses to which the assembly joints of electronic chips are subjected are becoming increasingly severe. As a result, thermal stresses acting on the electronic assembly, and particularly on the electrical interconnections, are becoming increasingly severe. The objective of this study is to create, characterize and optimize the structure and properties of a porous silver sintered joint using the design of experiments (DoE) method. Joints consisting of a porous network of silver particles are obtained, showing remarkable flexibility allowing for thermal stresses accommodation and having sufficient tensile strength to ensure a correct bonding of the components. Depending on the selected levels for the sintering process parameters, the microscopy analysis shows a transition of the mode of rupture from the silver layer to the intermetallic compounds forming at the interface with the substrate.**

***Keywords*— sintering; nano-silver paste; mechanical testing; microstructure**

I. INTRODUCTION

With the development of power electronics systems, there is an increasing need of having interconnection materials with properties that can ensure both a good mechanical strength of the bonding and high thermal/electrical conductivities in the assembly. So far, the lead-free solders have been considered as an attractive solution for die attach [1-3] but sintered joints based on nano-silver paste [4-6] are now considered as a replacement solution in the most demanding applications. The sintering technique proves indeed to be a promising solution, offering a thermal conductivity increased by many folds for the electronic packaging [7]. In addition, the sintered interconnect material can be manufactured with sufficient mechanical flexibility to accommodate the mismatch in coefficient of thermal expansion between the different components of the assembly. In power optics applications, the mechanical stresses can cause geometrical distortion in the active laser medium, and thus degrade the optical beam quality. It is then necessary to realize a flexible joint in such cases to solve the issue, which can be achieved by using low-pressure and moderate temperature conditions during the sintering process. However, evaluating quantitatively the effects of the process on the joint properties remains a challenge. It would of great use for the electronic manufacturing industry to have a systematic means to select precisely the process parameters for the desired properties.

The objective of this study is to fabricate sintered Ag joints on gold-plated copper and investigate, in relation with the chosen sintering conditions, their physical and mechanical properties. The analysis of the measurements is done by following a design of experiments (DoE), making it possible to estimate effects of process parameters, such as the heating rate and the applied pressure, on the mechanical properties of the fabricated samples, as well as on their microstructural features.

II. SAMPLE PREPARATION

A. Assembly silver precursor

Silver oxalates used in this study were obtained by the following process [7,8]. The Ag oxalates are decomposed into metallic silver below 200°C under controlled atmosphere, which allows for reduction of the metallic oxides. The chemical decomposition reaction occurs as follows:

$$Ag_2C_2O_4(s) \rightarrow 2Ag(s) + 2CO_2(g) \qquad (1)$$

During this reaction, the Ag oxalates reduce to highly reactive and pure nano-Ag particles after the organic content evaporates due to heat. At this stage, the spongy metallic nanometric grains replace the initial oxalate particles and are partially linked to each other by small metallic bridges. In order to make the process easier, a silver paste is made by mixing the decomposed silver oxalate powder with pure ethylene glycol in an ultrasonic bath. The obtained solder paste can then be deposited more easily on the surfaces to bond. The bonding process is finally realized by heating the assembly at a moderate temperature (≤ 300°C) as illustrated in Fig. 1a. The nanometric silver grains formed during the early stages of the oxalate decomposition possess a high propensity for sintering and, thus, only a relatively small bonding pressure is sufficient to enhance further the growth of the particles and the inter-particle bonds.

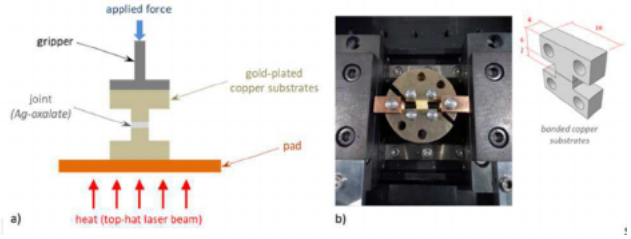

Fig. 1. (a) Schematic of the sintering setup for bonding copper parts, and (b) shear loading of a sintered sample under quasi-static conditions at room temperature.

B. Assembly substrate

This process is used to assemble several pairs of copper substrates. To ensure a good adhesion with the silver joint, the surfaces of the substrates to be bonded are gold-metallized beforehand [9]. The small-sized copper substrates have been fabricated with comparable dimensions to those of components used in microelectronics or optics packaging (bonded surfaces of 4×4 mm^2).

C. Assembly process

The sintering dwell time is fixed at 30 min and only two main controlling factors are made vary in the experimental design, namely the heating rate and the applied pressure. The experimental design consists of 6 different configurations as reported in Table 1 (D-optimal RSM DoE). Each configuration is replicated 5 times to have statistically representative results. All the specimens are tested under shear loading until rupture using a micro-tensile machine (Fig. 1b).

TABLE I.

Values of the controlling process parameters for the 6 configurations of the DoE		
Configuration	***Applied pressure (MPa)***	***Heating rate (°C/min)***
C1	0.5	20
C2	10	90
C3	7.5	20
C4	0.5	90
C5	4.5	60
C6	10	50

3. Results and Discussion

A. Mechanical characterization

From the load-displacement curves of the shear tests, the following mechanical properties have been extracted: maximal force or strength (N), elastic stiffness of the assembly (N/mm), critical elongation or displacement at rupture (mm) and work of fracture (mJ). It is observed that the values of all these properties increase significantly with the increase of the sintering pressure (Fig. 2). This effect is reinforced at higher values of the heating rate.

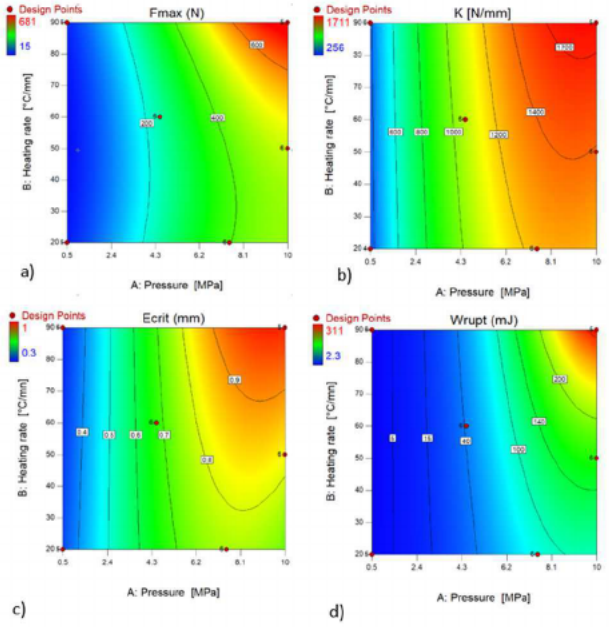

Fig. 2. Effects of the applied pressure and the heating rate on (a) maximal force, (b) elastic stiffness, (c) displacement at rupture, and (d) work of fracture.

The correlation coefficients between the different measured quantities have been estimated and are represented in Fig. 3a. It appears that all the mechanical properties are strongly correlated with each other. Having a tool to find the optimal process parameters leading to the best compromise in terms of mechanical properties is of great interest. For example, a high flexibility can be desired to accommodate the thermo-mechanical stresses under service, together with a good bonding strength of the microelectronic assembly. A specific relationship relating the maximal force and the elastic stiffness of the sintered silver joint is thus derived from the experimental data as represented in Fig. 3b. This diagram helps find the optimum corresponding to the lowest value of the elastic stiffness for compliance associated with a necessary and sufficient strength (maximal force) for the assembly.

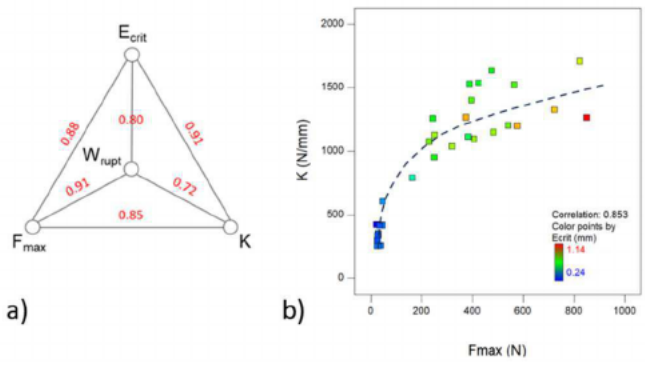

Fig. 3. a) Estimated correlations between the different mechanical properties, and (b) relationship between the elastic stiffness of the assembly and the strength of the sintered joint.

B. Microstructure of the bulk sintered Ag

The fracture surfaces are now investigated and the microstructural features of the sintered joints are compared. The effects of the process parameters are discussed by considering the two extreme configurations of the experimental design, associated respectively with the lowest sintering conditions C1 (20°C/min at 0.5 MPa) and the highest sintering conditions C2 (90°C/min at 10 MPa). In Figs. 4a and c, global views of the sintered joints after debonding are shown for the two configurations, showing a porous metallic network with typical micrometric porosities distributed more or less uniformly throughout the material. In Figs. 4b and d, close views of the same samples clearly exhibit that the porosity strongly differs depending on the sintering condition. The formation of necks (grain boundaries) is still at work in the case of the weak configuration (C1), which results in a network of large interconnected pores (open porosity). In the case of the strong configuration (C2), the reduction of porosity is far more important, indicating that an advanced stage of sintering has been reached due to a superior applied pressure combined with a higher heating rate.

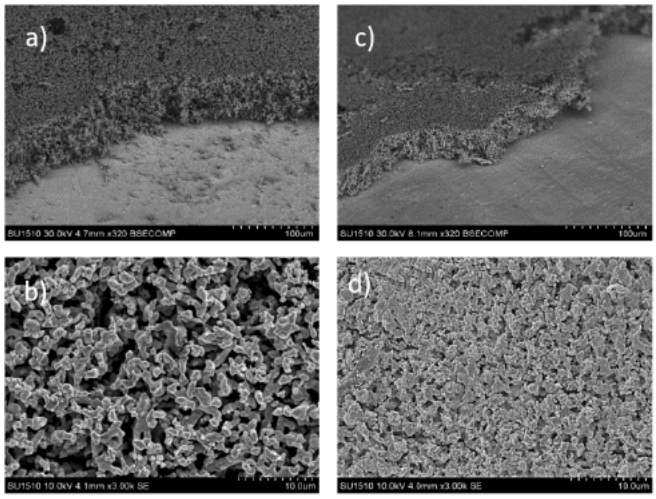

Fig. 4. Fig. 4: SEM Global and close views of the sintered silver joints after shear test achievement with (a)-(b) sintering conditions C1, and (c)-(d) sintering conditions C2.

Concerning the characteristics pertaining to particles morphology, the sintered joint in conditions C1 exhibits submicron-sized particles (~500 nm) with a good proportion of cubic-shaped particles which are typically associated with the earlier stages of the decomposition phase of silver oxalate precursors (Fig. 5a). It also appears that the material in the fracture zone does not display any plastic deformation. The sintered joint in conditions C2 displays, on the contrary, a deformed microstructure with particles elongated and plastically deformed after the shear loading. The particles in this case are also larger, over 1 micron in size (Fig. 5b).

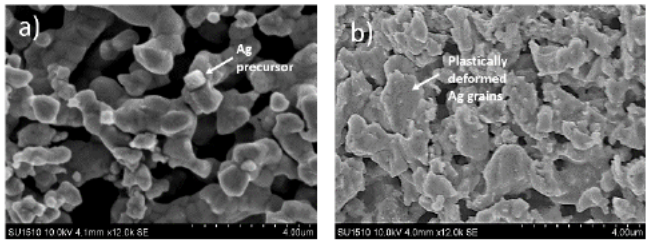

Fig. 5. SEM magnified views of the Ag particles after shear deformation for (a) sintering conditions C1, and (b) sintering conditions C2.

C. Analysis of the Ag/substrate junction

Analysis of the rupture surfaces shows that fracture occurs either inside the bulk sintered-Ag layer or at the interface with the gold-plated copper substrate, depending on the strength of the sintered material reached in the process. For the sintering conditions C1 (weakest configuration), large and thick chunks of the silver layer are found across the fracture zone (Figs. 6a-b), which indicates that the cohesive strength of the joint (strength of the bond between the sintered Ag particles) is weaker than the adhesion strength of the joint on the gold-plated copper substrate in these regions. Areas of the interface where silver was removed reveals that the junction layer that is expected to form by inter-diffusion of species (Au-Ag compound) is absent or hardly present. For the sintering conditions C2 (strongest configuration), no thick residues of the silver layer are observed on the fracture surface. The rupture appears to have occurred very close to the junction layer (formed from the gold metallization and the silver of the joint) or in the junction layer itself (Figs. 6c-d). The Ag particles are evenly spread over the fracture surface, exhibiting an elongated shape due to plastic shear deformation.

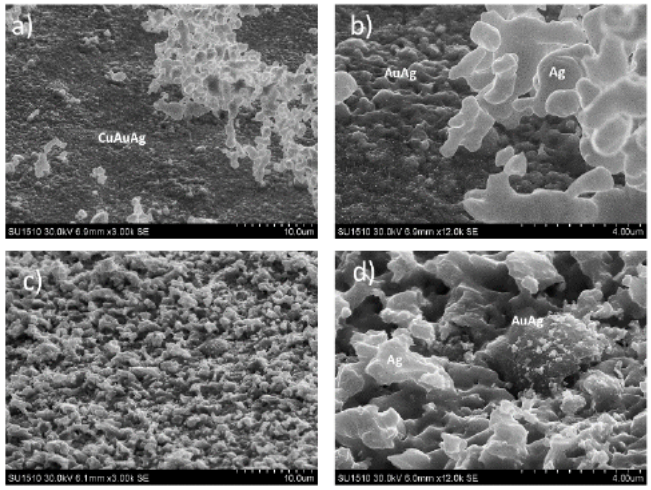

Fig. 6. SEM global and close views of the junction area between the sintered joint and the substrate for (a)-(b) sintering conditions C1, and (c)-(d) sintering conditions C2.

Cross-sections of the samples were also analyzed to have another view on the compounds forming at the sintered Ag/Au-plated Cu interface during the sintering process. Solid solution of the elements is achieved since gold is miscible in any proportions with both silver and copper, resulting in homogeneous phases [10]. The growth and final size of these compounds are dependent on the chosen levels of the process parameters during sintering, i.e. pressure and heat rate. The gold-silver (AuAg) solid solution, making the junction layer previously mentioned, is shown for both conditions C1 and C2 in Figs. 7a and 7b. The measured thicknesses associated with the two configurations are approximately 1.7 µm and 2.7 µm, respectively.

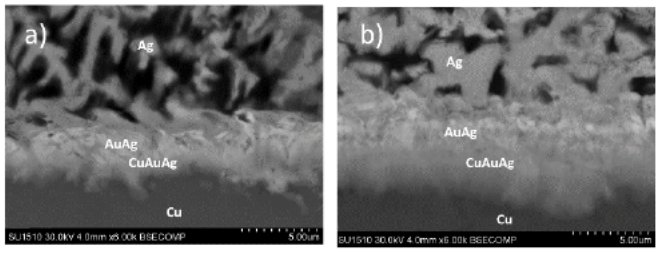

Fig. 7. Cross-section SEM views of the interface between the sintered silver layer and the gold-plated substrate for (a) sintering conditions C1, and (b) sintering conditions C2.

D. Microstructural measurements

Thicknesses of the joints in the different configurations were measured using the cross-sectional images. It can be seen in Fig. 8 that the obtained joint thickness is primarily determined by the sintering pressure. The heating rate has little or no effect and only a small decrease of thickness can be observed when the heating rate is changed from 20°C/min to 90°C/min. For the lowest applied pressure (0.5 MPa), the average thickness of the joints is 60±9 µm, while it is 36±5 µm for the highest pressure (10 MPa).

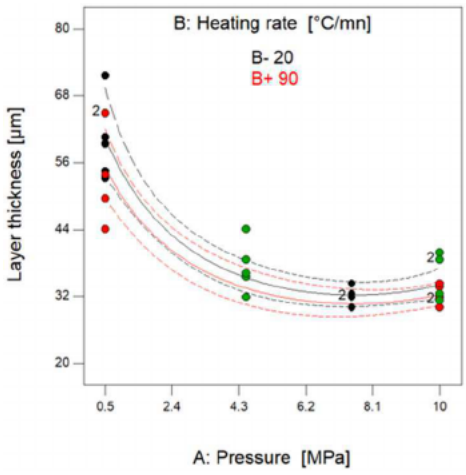

Fig. 8. Evolution of the sintered joint thickness with respect to the applied pressure and heating rate.

Using the ImageJ software [11], the relative density and the particle size distribution are measured for the sintered joints with sintering conditions C1 and C2 by processing their microscope images. The lowest sintering conditions (C1) leads to a highly porous sintered joint with open porosity. The measured value of the relative porosity is as high as 53%, and this is associated with relatively small grain sizes exhibiting a log-normal distribution (Figs. 9a-b). The grain sizes lie in the range between 0.45 µm and 1.25 µm, with an average size of 0.75 µm. The smallest silver grains obtained under these conditions are about the size of the silver precursors resulting from the silver oxalate decomposition (400 to 500 nm), which indicates that the sintering process remained in its first stages where the necks forms but grain growth is not significant. In the case of the highest sintering conditions (C2), image processing reveals a close porosity network with relative porosity dropping to 33% (Figs. 9c-d). The grain sizes, ranging from 0.9 µm to 2.5 µm, follow a Gaussian distribution and the average grain size with a value of 1.5 µm has doubled compared to that for the weak configuration.

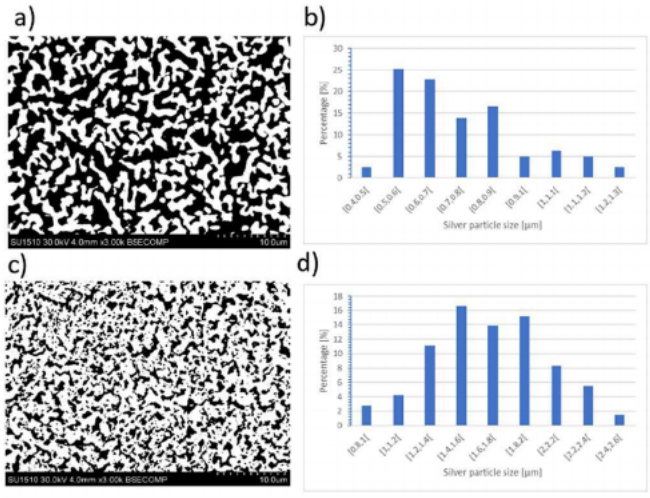

Fig. 9. Relative density and particle size distribution based on cross-section SEM images analysis, for (a)-(b) sintering conditions C1, and (c)-(d) sintering conditions C2.

Silver grain size is the measured physical characteristic that is the most dependent on the rate of temperature rise (Fig.10a), while porosity decreases mainly with pressure (Fig.10b). This effect is enhanced at higher values of the temperature rise rate, meaning that porosity can be decreased when the rate of temperature rise is increased under a high pressure, but it is little or not affected by the rate of temperature rise if a low pressure is applied.

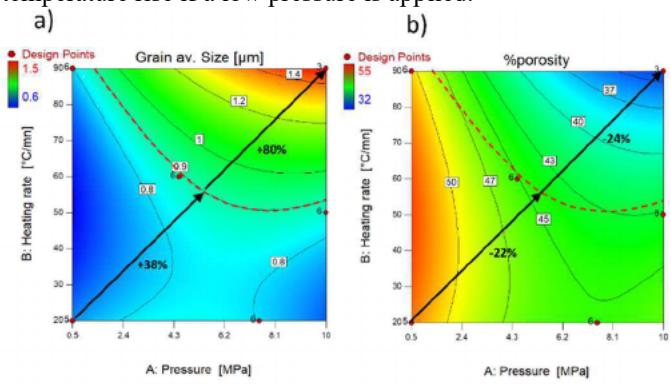

Fig. 10. Effects of the applied pressure and the heating rate on (a) the silver grain average size, and (b) the relative porosity of the sintered joint.

It can be established that the study area is clearly divided into two regions, following the 0.9µm grain size iso-line. Above this iso-value line, the increase in grain size with temperature rise rate and sintering pressure is twice as strong as that observed in the area below this iso value line. There is therefore a very strong acceleration of the growth of silver grains when this threshold is exceeded. The needed pressure for transitioning from the first regime of low grain size growth to the second regime of high grain size growth decreases considerably as the rate of temperature rise increases.

In terms of effects on the porosity rate, it is noticeable that, for both regions of the study area associated with the two grain size growth regimes, the decrease of the porosity rate with the rate of temperature rise and the sintering pressure remains approximately constant (Fig.10b). The silver particles get closer in the first regime (shrinkage), and they increase in size during the second regime (grain growth). These two regimes of transformation of the microstructure of the porous joints correspond typically to the first two stages of the sintering process. The first stage corresponds to the formation of necks between the silver precursor particles, due to rapid matter redistribution driven by interfacial tensions. This first stage continues until a local equilibrium of the interfacial tensions is established. Then, the "neck growth" stage starts, which corresponds to the interface migration under Laplace pressure gradient due to the surface curvature of the silver grains. This means that, in the transition zone between the first and second regimes, we are at the beginning of the grain size growth stage.

III. CONCLUSION

This study made it possible to map the mechanical and microstructural properties of porous sintered joints that can be obtained by varying 2 parameters of the sintering process: the pressure applied and the rate of temperature rise. The choice of the process parameters levels allowed us to cover all the stages of the silver powder sintering process. The most porous joints remain in the first sintering stage (formation of the necks), while the most dense sintered joints enter the phase of elimination of closed porosity. It was also possible to measure multiple mechanical properties for all

configurations of the sintered joint, and a law linking the joint mechanical strength to its flexibility has been established. This makes it possible, for a given application, to find the right compromise between the mechanical strength and the ability of the joint to deform elastically to best cope with the mismatch in thermal expansion in the multi-material system.

The measurements already carried out still need to be supplemented by additional measurements, in particular that of the Young's modulus of the porous sintered joints, using an atomic force microscope (AFM) for example. The thermal and electrical conductivities of these sintered joints also need to be simulated and, if possible, measured.

When all these experimental data are gathered, it will be possible in future works to simulate the behavior of electronic assemblies using these sintered joints subjected to thermal shocks and active cycling. The findings could then be compared with the results for some common solder joints, such as tin-based alloys, and help find the optimal process parameters for the sintered microstructure, i.e. the one that is the most reliable under harsh conditions of electrical and thermo-mechanical stresses.

REFERENCES

[1] M. Abtew, G. Selvaduray, Lead-free solders in microelectronics, Mat. Sci. Eng. R 27 (2000) 95-141.

[2] L. Benabou, V.N. Le, Z. Sun, P. Pougnet, V. Etgens, Effects of voids on thermal-mechanical reliability of lead-free solder joints, Fatigue Design & Material Defects (2014), https://doi.org/10.1051/matecconf/20141204026.

[3] V.N. Le, L. Benabou, Q.B. Tao, V. Etgens, Modeling of intergranular thermal fatigue cracking of a lead-free solder joint in a power electronic module, Int. J. Solids Struct. 106-107 (2017) 1-12.

[4] K. Suganuma, S. Sakamoto, N. Kagami, D. Wakuda, K.S. Kim, M. Nogi, Low-temperature low-pressure die attach with hybrid silver particle paste, Microelectron. Reliab. 52 (2012) 375-380.

[5] S. Fu, Y. Mei, G.Q. Lu, X. Li, G. Chen, X. Chen, Pressureless sintering of nanosilver paste at low temperature to join large area (≥100 mm2) power chips for electronic packaging, Mater. Lett. 128 (2014) 42-45.

[6] W. Guo, Z. Zeng, X. Zhang, P. Peng, S. Tang, Low-temperature sintering bonding using silver nanoparticle paste for electronics packaging, J. Nanomater., 2015. https://doi:10.1155/2015/897142.

[7] K. Kiryukhina, H. Le Trong, P. Tailhades, J. Lacaze, V. Baco, M. Gougeon, F. Courtade, S. Dareys, O. Vendier, L. Raynaud, Silver oxalate-based solders: New materials for high thermal conductivity microjoining, Scripta Mater. 68 (2013) 623-626.

[8] K. Kiryukhina, Pâtes à braser à base d'oxalate d'argent pour applications électroniques fortement dissipatives: de l'intérêt des particules nanométriques issues de la décomposition de l'oxalate d'argent, PhD Dissertation, University of Toulouse, 2014.

[9] K.S. Siow, Are sintered silver joints ready for use as interconnect material in microelectronic packaging, J. Electron. Mater. 43 (2014) 947-961.

[10] Handbook of Surfaces and Interfaces of Materials, H.S. Nalwa (Ed), Academic Press, 2001.

[11] C.A. Schneider, W.S. Rasband, K.W. Eliceiri, NIH Image to ImageJ: 25 years of image analysis, Nat. Methods 9 (2012) 671-675.